Science of the Total Environment xxx (xxxx) 172729

Contents lists available at ScienceDirect

Science of the Total Environment

journal homepage: www.elsevier.com

# Investigation of pyruvic acid photolysis at the air-liquid interface as a source of aqueous secondary organic aerosols

Xiao Sui [a], Bo Xu [b], Oleg Kostko [b], Xiao-Ying Yu [c,*]

[a] College of Geography and Environment, Shandong Normal University, Jinan 250358, China
[b] Chemical Sciences Division, Lawrence Berkeley National Laboratory, Berkeley, CA 94720, United States
[c] Materials Science and Technology Division, Oak Ridge National Laboratory, Oak Ridge, TN 37830-6136, United States

ARTICLE INFO

Editor: Hai Guo

*Keywords:*
Aqueous secondary organic aerosol (aqSOA)
Air-liquid interface
Photochemical aging
Pyruvic acid
SALVI
VUV SPI-MS

ABSTRACT

Pyruvic acid (PA) is a ubiquitous 2-oxocarboxylic acid in the atmosphere. Its photochemical process at the air-liquid (a-l) interface has been suggested as an important source of aqueous secondary organic aerosols. We investigated the photochemical reaction pathways of PA at the a-l interface using synchrotron-based vacuum ultraviolet single-photon ionization mass spectrometry (VUV SPI-MS) coupled with the System for Analysis at the Liquid Vacuum Interface (SALVI) microreactor. Results from mass spectral analysis and the determination of appearance energies (AEs) indicate that photolysis of PA can generate radicals, then they recombine with carboxylic acids and simple molecular oligomers. Furthermore, the preliminary products could form larger oligomers via radical reaction or esterification in the presence of hydroxyl and carboxyl functional groups. Mass spectral comparison shows that most photochemical reactions would complete within 4 h. The expanded photochemistry-driven reaction flowchart of PA is proposed based on the newly discovered products. Our results reveal that the interfacial PA photochemical reactions have different mechanisms from the bulk liquid due to the interfacial properties, such as molecular density, composition, and ion concentration. Our findings show that in situ mass spectral analysis with bright photon ionization is useful to elucidate the contribution of a-l interfacial reactions leading to aqSOA formation.

## 1. Introduction

Wide epidemiological studies have shown that exposures to fine particles are harmful to human health by increasing risks of respiratory and cardiovascular disease (Ito et al., 2019; Nel, 2005). Secondary organic aerosols (SOAs) are one of the main contributors to atmospheric fine particles. Many recent research efforts have focused on SOAs; and it is known that the composition of SOAs changes continuously with time and space (Qi et al., 2021; Stephanou, 2005). Process models are often built upon well-studied volatile organic compounds (VOCs) and their reactions pathways are important components (Tsui et al., 2017). Although SOAs have been studied extensively since the 1980s, there are still significant speculations about their formation due to the lack of mechanistic insights of interfacial chemistry and lack of understanding of their impacts on human health (Huang et al., 2014; Mellouki et al., 2015). Atmospheric SOAs could form via oxidation of VOCs or heterogeneous reactions of semi-volatile organic compounds (SVOCs) (Griffin, 2005; Lin et al., 2014; Tsui et al., 2017; Waxman et al., 2013). Recently, it was found that the uptake of VOCs and SVOCs at the air-liquid (a-l) interface is an essential pathway to generate aqueous secondary organic aerosols (aqSOAs), which could further convert to fine particles (McNeill, 2015). The a-l interfacial region changes at the molecular scale (i.e., density, ion composition, pH) that leads to different reactivities between the interface and bulk solutions (Pruyne et al., 2014).

Pyruvic acid (PA), an important atmospheric 2-oxocarboxylic acid, is ubiquitous in both gas and aqueous phase in the atmosphere (Church et al., 2021). Atmospheric PA mainly derives from multiphase isoprene oxidation and the interfacial oxidation reactions of aromatics compounds; and its sink is via photooxidation reactions with HO• and $HO_2$• radicals (Ervens et al., 2011). It is also known that aqueous PA could form organic polymers via photoinduced chemistry or dark aging by spontaneous self-assembly of PA. Such products contribute significantly to the aqSOA budget (Perkins et al., 2016; Rapf et al., 2017b). Particularly, the main sink of atmospheric PA is photochemical reactions, and these processes are believed to occur in the multiple phase and interfacial region, such as the grain boundaries of ice/glass state and the inter-

* Corresponding author.
*E-mail address:* yuxiaoying@ornl.gov (X.-Y. Yu).

https://doi.org/10.1016/j.scitotenv.2024.172729
Received 28 January 2024; Received in revised form 22 April 2024; Accepted 22 April 2024
0048-9697/© 20XX

Note: Low-resolution images were used to create this PDF. The original images will be used in the final composition.

face of air bubbles or water (Li et al., 2023; Rapf et al., 2017a). The aqueous PA concentration in atmospheric bulk conditions (i.e., in cloud and fog droplet) is approximately10 μM to 20 mM. The photochemical products are mainly small molecules, such as carboxylic acid acetals and/or dimers via multistep oxidation, aldol addition, and condensation reactions. Concentrations like those in the atmospheric conditions are mainly used to study PA reaction mechanisms in the bulk phase (Petters et al., 2020). However, the concentration at the air-liquid interface will be enriched with droplets drying under solar irradiation, which could lead to low-volatility oligomer formation by radical reactions. Also, unsaturated dimers can contribute to SOA formation (Guzma'n et al., 2006; Lim et al., 2010). The chemical mechanisms of PA generate various interests because PA can be an aqSOA model system to represent more complex organic molecules in the atmosphere, such as the atmospheric processing of aromatic compounds emitted by biogenic and anthropogenic sources (Zhang et al., 2022). Thus, determination of photochemical processes at the a-l interface is essential to investigate how PA contributes to aqSOA at the aerosol surface. Nevertheless, laboratory results are scarce because it is experimentally challenging to probe the surface reactions of aerosols and droplets involving the liquid phase directly. Using surface sensitive instruments like SEM (scanning electron microscope), XPS (X-ray photoelectron spectroscopy), and ToF-SIMS (time-of-flight secondary ion mass spectrometry) and bulk phase mass spectrometry require ultrahigh vacuum. Thus, it is difficult to study the liquid surface directly because liquid will evaporate quickly and liquid will dry up in vacuum (Du et al., 2017; Yu, 2020; Zhou et al., 2016).

Synchrotron based single-photon ionization mass spectrometry (SPI-MS) with bright vacuum ultraviolet (VUV) photons has been widely used to investigate chemical systems and their dynamics. (Kostko et al., 2016; Sui et al., 2021a). Compared with other ionization analyzers, like charged particles and ions impact, VUV SPI-MS offers “soft” ionization to detect organic molecules with fewer fragments (Gerald L. Gasper et al., 2010). Besides, the ionization energies (IEs) can be used to improve the precision of chemical compound identification by comparing the known IEs and their molecular signals in the mass spectrum (Kostko et al., 2016). Several recent studies have shown that the air – liquid (a-l) interface can be approximated using the vacuum – liquid (v-l) interface to study reaction mechanisms at the interface. This is because if the evaporation rate of liquid is slow enough, the composition and temperature during analysis in the main chamber will not significantly change and the near surface liquid can compensate for the evaporation (Lee et al., 2016; Winter and Faubel, 2006). Also, if the residence time of the solvent is long enough, the solute can diffuse to the surface from the bulk to build up the surface excess and its concentration will not reduce along with evaporation (Lee et al., 2015). Thus, detection carried out in vacuum and under the a-l equilibrated conditions will return consistent results. Another advantage is the signal to noise ratios in vacuum are higher than in the gas phase, because the photoelectrons will be scatted by gas molecules under higher pressure than the pressure in the TOF-MS ion source. (Lee et al., 2016). Based on this principle, established techniques used in atmospheric chemistry include the liquid microjet or droplet trains coupled with high-vacuum XPS, which has been used to study chemical composition and properties of the v-l interface (Brown et al., 2009; Lee et al., 2016; Lewis et al., 2011; Pruyne et al., 2014; Seidel et al., 2011).

Recently, our group has demonstrated that the a-l interfacial reactions of relevance to aqSOAs can be studied using a unique vacuum compatible system for analysis at the v-l interface (SALVI) (Sui et al., 2017a; Zhang et al., 2019a; Zhang et al., 2019b). Compared with the microjet approach, molecules evaporated from the small aperture of the SALVI microreactor have a stable surface for probing. This helps meet the evaporation rate and residence time requirements, and it is suitable for multimodal imaging and analysis (Yang et al., 2011; Yu, 2020). The SALVI microfluidic reactor has been integrated to ToF-SIMS and VUV SPI-MS recently to study environmental processes at the a-l interface (Griffith et al., 2013; Komorek et al., 2020; Sui et al., 2017a; Zhang et al., 2022; Zhang et al., 2019b).

Herein, we present the investigation of PA photolysis reactions, a model system known to produce SOAs (Griffith et al., 2013). The photochemical reactions at the a-l interface are approximated by the v-l interface in this work based on the related discussion above and our recent results (Sui et al., 2021a; Sui et al., 2017a). The photochemical reaction pathways of PA have been investigated and expanded based on detection of new species in the first study of pyruvic acid aqueous photolysis using VUV-SPIMS. Specifically, key products and reactants were identified by mass spectral analysis and confirmed using their corresponding appearance energies (AEs). Our results provide new understanding of PA photochemistry that occurs at the a-l interface contributing to aqSOAs in the Earth's atmosphere.

## 2. Materials and methods

### 2.1. SALVI fabrication

SALVI devices used in this work were fabricated using soft lithography. More details were provided in previous studies (Yu et al., 2013; Zhou et al., 2016). Briefly, each microfluidics device has a 200 μm wide and 300 μm deep microchannel in a polydimethylsiloxane (PDMS) block. The microchannel was covered by a 1.5 × 1.5 $mm^2$ and 100 nm thick silicon nitride (SiN) membrane (Norcada, Edmonton, Canada) with good transmittance supported on a silicon frame of 7.5 × 7.5 $mm^2$ and 200 μm thick (Haruta et al., 2019). After microfluidics fabrication, two micropores (2 μm in diameter and 100 μm apart, Fig. 1b) were milled on the center of the channel using the scanning electron microscopy - focused ion beam (SEM-FIB, ThermoFisher Helio Dual Beam) instrument to allow evaporation of molecules in vacuum stably and provide high intensity in spectra based on our previous studies (Komorek et al., 2018; Komorek et al., 2020).

### 2.2. Sample preparation

To better simulate aqSOA formation at the aqueous interface, PA (98 wt%,) was acquired from Sigma-Aldrich, St. Louis, MO, USA. Pyruvic acid solutions were prepared to be 0.1 M using deionized water (DI water, 18.2 MΩ, Barnstead water purification system, Nanopure diamond) as an atmospheric model system (Fu et al., 2018; Guzma'n et al., 2006; Reed Harris et al., 2017). The Henry's law constant is 4.0 × $10^7$ M/atm for 0.1 M PA, which is between the constant for pyruvic acid concentration in cloud or fogwater (3.1 × $10^5$ M/atm) and for its saturation concentration as observed in the atmosphere (2.0 × $10^9$ M/atm) (Reed Harris et al., 2014). (The PA concentration used in this work was used to study droplet evaporation process (Reed Harris et al., 2017). It should be noted that impurities like lactic acid, acetic acid, parapyruvic, and zymonic acids could be generated inevitably from the self-reaction of PA under dark condition during storage (Reed Harris et al., 2017). Thus, dark reaction of PA may also contribute to products that may be regarded as photochemical reactions, for instance, subsequent oligomerization of lactic acid and acetic acid or decarboxylation reactions of zymonic acids. It is important that the freshly purified PA should be used to minimize interference from dark reactions. However, those impurities were not observed in the spectrum, which indicated the effects of impurities were minimized during sample preparation and VUV SPI-MS analysis.

To minimize the PDMS interferences, the SALVI devices were baked in a vacuum oven (Fisher, Model 282 A, Waltham, MA, USA) overnight at 65 °C and the microchannel was thoroughly flushed with DI water three times before usage. 100 μL solutions containing 0.1 M PA was injected into the microchannel using a syringe pump at a rate of 10 μL/min. Afterwards, a Hg—Ar UV lamp (ORIEL, lamp model 6035, USA)

CORRECTED PROOF

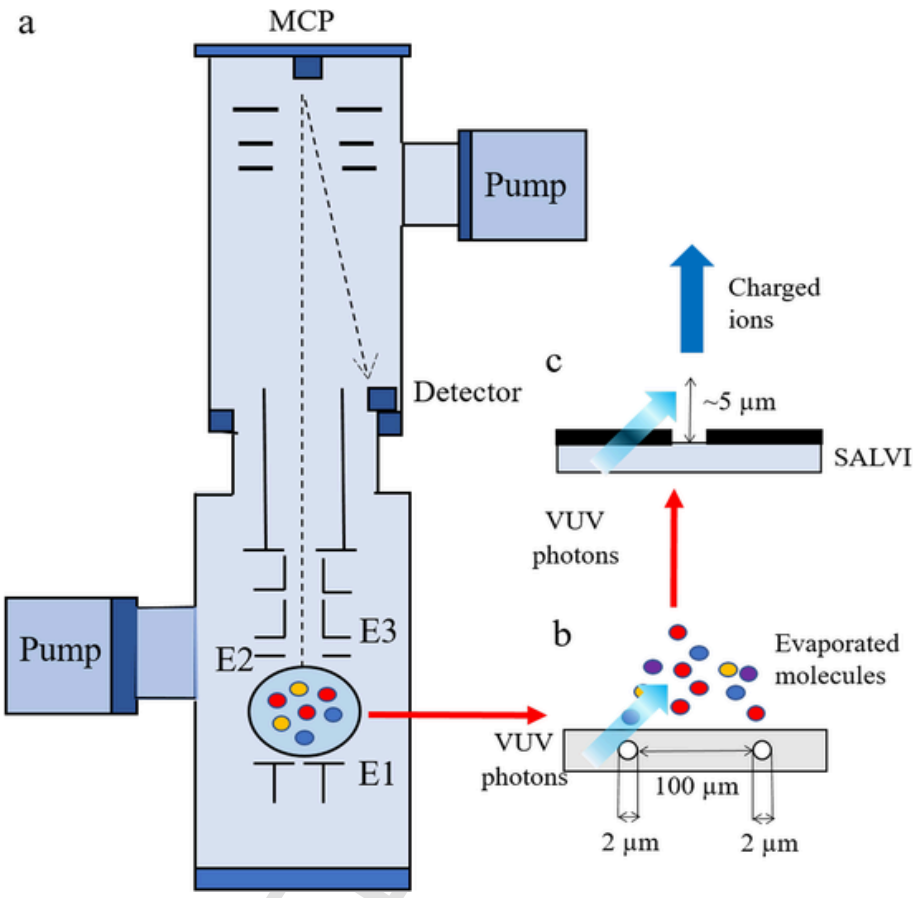


**Fig. 1.** The experimental schematics of pyruvic acid UV aging: a) the charged ions detected by reflectron time-of-flight mass spectrometry. MCP: microchannel plate. E1: electrode 1, E2: electrode 2, and E3: electrode 3; b) the cartoon showing of cross-sectional view of Analysis at the Liquid Vacuum Interface (SALVI); and c) the position of the VUV photon flux relative to evaporated molecules above the device.

was used for illumination (Reader et al., 1996). The distance between the microfluidic device and the UV lamp was kept at 10 cm to simulate the photochemical process in the atmosphere (Fu et al., 2018; Sui et al., 2017b; Zhang et al., 2019b). This wavelength distribution, is effective for photolysis of PA reactions at the aqueous surface, namely in the range of 300 to 380 nm as shown in several previous works by different groups (Fu et al., 2018; Guzman et al., 2006; Rapf et al., 2017a; Reed Harris et al., 2017). As to the wavelengths $\lambda < 300$ nm, PA could be excited to S2 $^1(\pi, \pi^*)$ state. When the output extends to 220 nm, the products generated from PA photolysis are in good agreement compared to those when 220–300 nm radiation is filtered (Rapf et al., 2017a). This result indicated photochemical reactions should follow the same pathways whether $\lambda$ is $<300$ nm or $\lambda$ is between 300 and 380 nm. It was reported that no additional pathways were triggered from S2 state (Rapf et al., 2017b). In the UV aging process, the photolysis of 0.1 M PA lasted for 1 h., 4 h., and 24 h. in the microchannel. The dissolved oxygen was protected within the microchannel during photolysis before products detection using VUV SPI-MS. The irradiance setting and absorption cross sections of PA were illustrated in Fig. S1.

### 2.3. VUV SPI-MS setup

After the photochemical aging treatment in the microchannel adjacent to the endstation, the SALVI device was brought to the beamline and attached to the bottom electrode of the ion optics module immediately (Fig. 1b). The measurements were conducted using a SPI-MS coupled with a three-meter VUV monochromator at the 9.0.2 Chemical Dynamics Beamline at the Advanced Light Source (ALS) at the Lawrence Berkeley National Laboratory (Ahmed and Kostko, 2020). The top of the device was elevated manually, and the SiN membrane was set about 5 mm under the VUV photon flux by optimizing the height of the mass spectrometer prior to data collection in each experiment (Komorek et al., 2018; Sui et al., 2021a). The microchannel plate (MCP) voltage was tuned to optimize signals from the evaporated products. Finally, the ionized molecules were collected and detected by the ToF mass spectrometer (Fig. 1a).

The molecules formed at the aqueous surface were estimated to evaporate at a rate of $10^8$ /cm$^2$/s from the two holes milled on the SiN membrane for there are approximately $10^8$ molecules entry the vacuum chamber pre square millimeter and per second using a custom code (Komorek et al., 2018; Yang et al., 2011). Meanwhile, the surface tension across the apertures allows the liquid to stay within the aperture in the microchannel and not lose vacuum (Yang et al., 2011). It took about 20 min to pump the chamber to the desirable vacuum of $10^{-7}$ Torr after the SALVI device containing liquid sample was loaded to the bottom electrode (E1). The chamber vacuum was maintained at the $10^{-7}$ Torr during experiments without modification of the instrument by using the existing vacuum pump. The photon energies were set to scan from 9.5 to 12.7 eV for all samples with a 0.1 eV step to obtain the photoionization efficiency (PIE) curve of key products by integrating the peak intensities at each photon energy. Data were collected in the positive ion mode in the existing setup (Komorek et al., 2018; Sui et al., 2021a). All samples were repeated twice to verify results and the datasets were named group A and group B, respectively. The experimental data showed good repeatability as shown in Fig. S2.

CORRECT

The mass to charge ratio ($m/z$) range of SPI-MS was set to 0–600 for 24 h. and 4 h. UV aged samples; and 0–300 for the 1 h. UV aged PA and fresh PA solution samples. These samples were analyzed in two different beam trips due to time constraints on the beamtime. Although the $m/z$ range was different due to the instrument setup between the two trips, the observed key products for the mass range lower than $m/z$ 300 were consistent between the two sets of experiments (Fig. S3). Chemical reactions and products detected were not influenced by the instrument setup as expected. The results were comparable between two different trips. Although, the mass ranges were set up slightly differently, this is why the mass spectral ranges were not identical for comparison purpose. In order to reduce differences arisen from possible interferences of system variations over time, we used normalized data in this work. The 24-h. UV aged sample was not intentionally prepared. Due to beamline technical difficulties, data acquisition was not possible until 24 h after sample preparation. For completeness, the 24-h. sample was included as a reference.

### 2.4. Data analysis

The SPI-MS mass calibration was performed according to the known chemical compounds, e.g., water, oxygen, or rare gases (Komorek et al., 2020). Mass spectra were plotted and integrated in Origin®. During the VUV SPI-MS analysis, a continuous wave ion beam was converted to a pulsed one to have access to more photons (Kostko et al., 2016). The spectra would be affected by pulsing: for small molecules, higher relative energy is acquired which results in narrower peaks, and the situation is the opposite for larger molecules. As a result, the mass resolution was not uniform over the mass range. Thus, unit mass at the peak center was used for peak identification. The peak centers could be slightly different at different photon energies for a particular compound. However, it should not affect peak identification based on the unit mass. For example, the ions detected at 10.7 eV and 12.0 eV were consistent, shown in Fig. S2.

The AEs of key products were all smaller than 12.0 eV according to the analysis results. However, the compounds would dissociate under high photon energies, which results in decreasing counts and increasing fragments. Besides, the species may be less well-defined at lower IEs because fewer ions may form characteristic peaks. Therefore, mass spectra at 12.0 eV were chosen for peak identification. The first point on the PIE curve which corresponds to the increase from the background signal was determined to be the AE of the molecule. On the premise of assuring the accuracy of experimental data, the lowest photon energy was selected to be 9.5 eV due to beamtime constraints, slightly lower than the ionization energy of PA reported in NIST Chemistry WebBook (https://webbook.nist.gov/chemistry/). This setup was similar to a previous study to acquire comparable information (Rapf et al., 2017a). When the counts of the PIE curves deviate from the baseline at the minimum photon energy, the AEs were assigned to be $<9.5$ eV according to the definition of AEs (Ahmed and Kostko, 2020; Kostko et al., 2016). The measured AEs and PIE curves were compared with literature reported IE values and PIE curves to determine if they were in agreement or not. There was a difference in the total counts of these samples, because each device had slightly different height between the UV photon beam due to their location, manual height adjustment, and instrument parameters between two different beamline visits. Normalized spectral results were used to reduce this kind of uncertainties as show in Figs. 3 and S3.

During the VUV SPI-MS analysis, a continuous wave ion beam is converted to a pulsed one. The resulting mass spectra are affected by the pulsing and the resolution is not uniform over the mass range. Thus, only unit mass was used for peak identification (Sui et al., 2021a; Sui et al., 2021b). However, peak separation is not a problem because peak positions can be identified to two decimal places of accuracy. In this study, three approaches were used to improve the likelihood of peak identification. First, peaks that have distinctly higher intensities than adjacent peaks were selected as key products, reactants, or fragments of them. Second, the identities of peaks were proposed based the existing knowledge of the PA photolysis pathways. Furthermore, AEs acquired from PIE curves were carried out to determine the chemical composition by comparing values with known IEs. For the products that AEs and/or structures that have not been reported in previous studies, the structure was deduced by considering the spectrum, PIE curve, and the most likely reaction pathways based on knowledge of the system and known literature (as shown in Table 1).

## 3. Results and discussion

### 3.1. VUV SPI-MS spectra analysis

Peaks were chosen based on the following criteria according to our previous publication: 1). the magnitude of a peak was significantly higher than its neighboring peaks; 2). the intensity of the peak in the mass spectrum was at least 3 times higher than the base lines; and 3). product peaks identified in previous papers relevant to PA photolysis were included in this study (Fu et al., 2018; Sui et al., 2017a). The mass spectra of the 4 h. UV aged PA samples at 12.0 eV were depicted in Fig. 2. Similarly, the twice repeated samples at 12.0 eV and 10.7 eV were compared in Fig. S2 respectively. These results show a similar distribution of detected peaks, indicating that the in situ VUV SPI-MS analysis has good reproducibility between two replicate specimens across different photon energies. The observed interference peaks from PDMS were evaluated in Table S2 and Fig. S5. The results show that the PDMS interferences only count 4.48 % of total signals, which indicates that their relative abundances do not interfere with the peak identification.

The mass resolution is inconsistent in the spectra because a continuous wave beam is converted to a pulsed one. Therefore unit mass is used for peak identification and presentation (Sui et al., 2021a). The highest counts used for peak identification could be detected in different forms (shown in Fig. S6). The observation of parent, deprotonated, and protonated ions was likely caused by the proton-transfer process during VUV analysis (Bell et al., 2013). PA and its deprotonated fragment are identified from mass spectral analysis, such as $m/z$ 88 (PA molecule) and $m/z$ 87 (deprotonated PA). Other peaks, such as $m/z$ 31, 33, 35, 43, 45, and 62 (PA fragments), are produced from reactive ion–molecule collisions followed by unimolecular decomposition from reactants and products (Ahmed and Kostko, 2020). Similarly, $m/z$ 105 (PA diol) was observed in both the UV aged solution and the as-prepared fresh PA solution without any UV irradiation (Fig. S3). As expected, these reactant peaks have higher intensities in the sample without UV illumination except for $m/z$ 87. Several peaks including $m/z$ 42, 71, and 82 observed in the UV treated solution are difficult to assign based on the known pathways of PA photolysis. Also, higher intensities of these species were observed at higher energies (see Fig. S4). Thus, it is postulated that these peaks are fragments related to the reactant and reaction products. By comparing mass spectral results, a series of product peaks were identified in the samples after 1 h., 4 h., and 24 h. UV treatment as follows. First, the products form due to photolysis of PA, such as acetaldehyde ($m/z$ 44) and acetic acid ($m/z$ 60). Second, radical reaction products include 3-hydroxy-5-methylfuran2(5H)-one ($m/z$ 113 $C_5H_5O_3^+$), 3- hydroxy-2-ethyl-4-pyranone ($m/z$ 139 $C_7H_7O_3^+$), 2-hydroxy-2-(2-oxopropoxy) acetic acid ($m/z$ 147 $C_5H_7O_5^+$), dimethyltartaric acid ($m/z$ 177 $C_6H_9O_6^+$), 3-hydroxybutane-1,2,3-tricarboxylic acid ($m/z$ 206 $C_7H_{10}O_7^+$), and hydroxycitric acid ($m/z$ 208 $C_6H_8O_8^+$). Third, cross photoreaction products of pyruvic acid and glyoxylic acid, for instance C6-cross intermediate ($m/z$ 191 $C_6H_7O_7^+$), are present. Fourth, oligomer products consist of $m/z$ 159 $C_6H_7O_5^+$, $m/z$ 256 $C_{10}H_8O_8^+$, $m/z$ 306 $C_{10}H_{10}O_{11}^+$ and $m/z$ 340 $C_{10}H_{12}O_{13}^+$. The counts of larger products ($m/z > 100$) in the 24 h. and 4 h. UV samples are higher than the shorter time-stamped sample, indicating that longer photochemical

CORRECTED PROOF

**Table 1**
Key products in 4 h. UV aging of pyruvic acid at 12.0 eV.

| $m/z$, obs [a] | $m/z$, the [b] | Formula | Chemical names | AEs(eV) | refs | Suggested structures |
|---|---|---|---|---|---|---|
| 42 | 42.04 | $CH_2CO^+$ | Pyruvic acid fragment | 10.3[c] | – | – |
| 44 | 44.05 | $CH_3CHO^+$ | Acetaldehyde | 10.7 | (Altieri et al., 2006) | |
| 60 | 60.05 | $CH_3COOH^+$ | Acetic acid | 10.3 | (Griffith et al., 2013) | |
| 88 | 88.06 | $C_3H_4O_3^+$ | Pyruvic acid | 10.1 | – | |
| 105 | 105.07 | $C_3H_5O_4^+$ | Deprotonated pyruvic diol | < 9.5[c] | This study, (Griffith et al., 2013) | 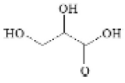 |
| 113 | 113.09 | $C_5H_5O_3^+$ | Deprotonated 3-hydroxy-5-methylfuran2(5H)-one | 10.1[c] | This study, (Rapf et al., 2017a) | 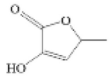 |
| 139 | 139.13 | $C_7H_7O_3^+$ | Deprotonated 3- hydroxy-2-ethyl-4-pyranone | < 9.5[c] | This study | |
| 147 | 147.11 | $C_5H_7O_5^+$ | 2-Hydroxy-2-(2-oxopropoxy)acetic acid | 11.8[c] | This study, (Xia et al., 2018) | 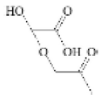 |
| 159 | 159.12 | $C_6H_7O_5^+$ | Oligomer | 9.8[c] | This study, (Fu et al., 2018) | 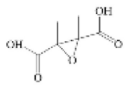 |
| 177 | 177.13 | $C_6H_9O_6^+$ | Protonated dimethyltartaric acid | < 9.5[c] | This study, (Fu et al., 2018) | 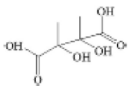 |
| 191 | 191.12 | $C_6H_7O_7^+$ | C6-cross intermediate | < 9.5[c] | This study, (Xia et al., 2018) | 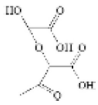 |
| 206 | 206.15 | $C_7H_{10}O_7^+$ | 3-Hydroxybutane-1,2,3-tricarboxylic acid | < 9.5[c] | This study | 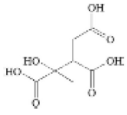 |
| 208 | 208.12 | $C_6H_8O_8^+$ | Hydroxycitric acid | < 9.5[c] | This study | 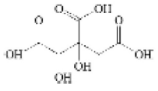 |
| 256 | 256.17 | $C_7H_{12}O_{10}^+$ | Oligomer | < 9.5[c] | This study | 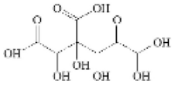 |
| 306 | 306.22 | $C_{10}H_{10}O_{11}^+$ | Oligomer | 9.8[c] | This study | 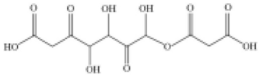 |
| 340 | 340.20 | $C_{10}H_{12}O_{13}^+$ | Oligomer | 9.6[c] | This study, (Fu et al., 2018) | 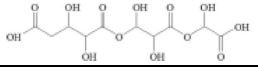 |

[a] Observed $m/z$.
[b] Theoretical $m/z$ from the NIST Chemistry WebBook.
[c] AE values determined in this work.

processing time is a factor to facilitate oligomer formation. Furthermore, few oligomers and oxoacids (i.e., $m/z$ 177, 206, 208) were detected in the PA solution due to the radicals reaction formed by self-assembly of PA as seen in Fig. S3 (Rapf et al., 2017b).

It was noted that the peaks have similar intensities between 4 h. and 24 h. samples. As discussed in Section 2.4, the 24 h. UV sample could represent the case of extremely long photolysis. Thus, the spectral comparison results imply that most PA photolysis reactions would finish within several hours. PA photolysis was assumed to be a first-order reaction (Reed Harris et al., 2016), and the reaction rate constants of PA photolysis can be estimated to be approximately $6.94 \times 10^{-5}\ s^{-1}$ at the liquid surface, assuming reactions are complete within 4 h. Observation of key reactants and products in this study are summarized in Table 1. Compared with static ToF-SIMS results (Fu et al., 2018), some radical reaction products and oligomers, such as $m/z$ 113, 159 and 340, were in agreement. However, smaller molecules, such as acetaldehyde ($m/z$ 44), acetic acid ($m/z$ 60), and PA molecule, were not observed using static ToF-SIMS. This discrepancy could be attributed to the fact that dry samples were analyzed using conventional static SIMS.

Besides the products validated by previous studies (Table 1), newly discovered products including $m/z$ 139 $C_7H_7O_3^+$, $m/z$ 206 $C_7H_{10}O_7^+$, $m/z$ 208 $C_6H_8O_8^+$, $m/z$ 256 $C_{10}H_8O_8^+$, and $m/z$ 306 $C_{10}H_{10}O_{11}^+$ were

CORRECTED PROOF

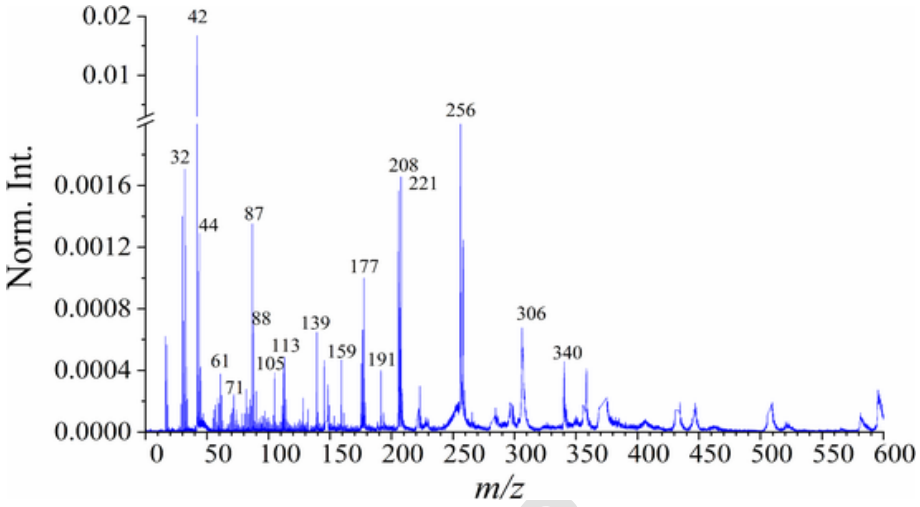


**Fig. 2.** The VUV-SPIMS spectrum of the 4 h. UV aged solution at PIE of 12.0 eV.

detected by VUV SPI-MS at 12.0 eV. This is because we used a unique vacuum compatible microfluidic interface to make it possible to study the air-liquid interface (Zhang et al., 2022). Overall, in situ VUV SPI-MS and ToF-SIMS showed different kinds of products formed via PA photochemical aging at the a-l interface. This finding indicates that new reaction pathways of PA UV aging should be proposed based on VUV SPI-MS coupled with SALVI.

### 3.2. AE determination

AE values of key products obtained were presented in Fig. 3 and Table 1 based on the PIE curves of the 4 h. UV aging sample and verified with other available data. Meanwhile, AEs derived from the 24 h. UV aging sample and PIE curves of the corresponding products were depicted in Fig. S7. The PIE curve shapes were in good agreement, indicating the detected AEs depended on the inherent chemical species and structures, not affected by aging time. As to smaller molecular products, i.e., *m/z* 44, *m/z* 60, and *m/z* 88, their molecular structures can be determined directly from the known PIE curves and IEs. Specifically, the AE for *m/z* 44 (shown in Fig. 2b) was 10.7 eV, which is identified as acetaldehyde based on previous studies (Church et al., 2021; Samanta et al., 2021). The AEs for *m/z* 60 (Fig. 3c) and *m/z* 88 (Fig. 3d) were 10.3 eV and 10.1 eV, respectively, which are identified as acetic acid and PA molecules based on the known PA photochemical pathways and NIST Chemistry WebBook (https://webbook.nist.gov/chemistry/) (Rapf et al., 2017a). The PIE curve of *m/z* 42 (Fig. 3a) and *m/z* 105 (Fig. 3e) had an AE of 10.3 eV and < 9.5 eV, respectively. They were assigned as PA fragments and PA diol according to past studies (Rapf et al., 2017a; Samanta et al., 2021).

Additionally, the AEs for *m/z* 113 (Fig. 3f) and *m/z* 139 (Fig. 3g) are 10.1 eV and < 9.5 eV. The products of *m/z* 139 were not reported in previous studies. In a recent study, *m/z* 113 3-hydroxy-5-methylfuran2 (5H)-one was reported as a product of pyruvic acid reactions (Fu et al., 2018). Based on the similarities of chemical structures and PIE results between *m/z* 113 and *m/z* 139, the new product *m/z* 139 was proposed as 3-hydroxy-2-ethyl-4-pyranone. The AEs for *m/z* 147, *m/z* 177, *m/z* 206 and *m/z* 208 were determined to be 11.8 eV, < 9.5 eV, < 9.5 eV and < 9.5 eV, respectively, shown in Fig. 3h, g, l and m. These were identified as radical reaction products.

Furthermore, the AEs of oligomers formed at the a-l interface were determined as the following: *m/z* 159 $C_6H_7O_5^+$ 9.8 eV (Fig. 3i), *m/z* 256 $C_{10}H_8O_8^+$ < 9.5 eV (Fig. 3n), *m/z* 306 $C_{10}H_{10}O_{11}^+$ 9.8 eV (Fig. 3n) and *m/z* 340 $C_{10}H_{12}O_{13}^+$ 9.6 eV (Fig. 3p). It is worth noting that the PIE curves and AEs of some oligomer products (i.e., $C_{10}H_8O_8^+$, $C_{10}H_{10}O_{11}$, $C_{10}H_{12}O_{13}^+$) present similar features, which implies that those oligomers share semblable molecular structures and functional groups. Combined with spectral analysis and AE determination, the possible structures of key products of PA UV aging are depicted in Table 1. These results show that the interfacial products could be assigned more precisely by VUV SPI-MS based on the deterministic *m/z* values and AEs.

### 3.3. The a-l interfacial reaction pathways

On the surface of water, PA in the gas phase can form pyruvate ions by giving a proton to neutral water molecules, which causes the increased acidity and the promotion of PA dissociation (Eugene et al., 2018). Correspondingly, the pyruvate ion peak (*m/z* 87) in the UV irradiated solution was observed with high intensity. However, the peak intensity of pyruvate ions in non-UV samples is low, indicating that the transformation process mainly occurs under UV irritation at the a-l interface. The pH of 0.1 M PA bulk aqueous samples ranges from 1.79 to 1.82. At the interface, a similar acidic condition is likely based on the fact that similar intensities of carboxylic acid and oligomers were observed in both bulk and interface samples detected using ToF-SIMS (Fu et al., 2018). More oligomers observed in 4 h. than 1 h. UV samples in this work, which implies that an increasing acidity at the aqueous surface. Because as larger oligomers are formed more abundantly, acidity will increase (Gao et al., 2004). As one of the few VOCs that degrade by solar radiation rather than free radicals, PA could be decarboxylated to form acetaldehyde and acetic acid in both gas and condensed phases via primary UV photodissociation (Reed Harris et al., 2017; Samanta et al., 2021). This photolysis pathway could also appear at the a-l interface verified by our results. Another reaction path is cross photoreaction, which is essentially a radical reaction that starts from the singlet excited state PA* that is activated by light ($\lambda$ > 300 nm) (Griffith et al., 2013). Research showed that glyoxylic acid (GA) together with PA could form cross photolysis product in aqueous aerosols (Xia et al., 2018).

Another proposed pathway was that PA and GA can form cross-reaction products with higher oxygen to carbon (O/C) ratios (i.e., O/C 0.83–1.20) via photolysis (Xia et al., 2018). GA could be generated from PA under the irradiation of UV light. GA was observed by ToF-SIMS in a recent report (Fu et al., 2018), but it was not detected by VUV SPI-MS in this study. Thus, the observation of cross photolysis products (e.g., *m/z* 147, oxo-C5 cross-product and *m/z* 191, precursor of oxo-C6

UNCORRECTED PROOF

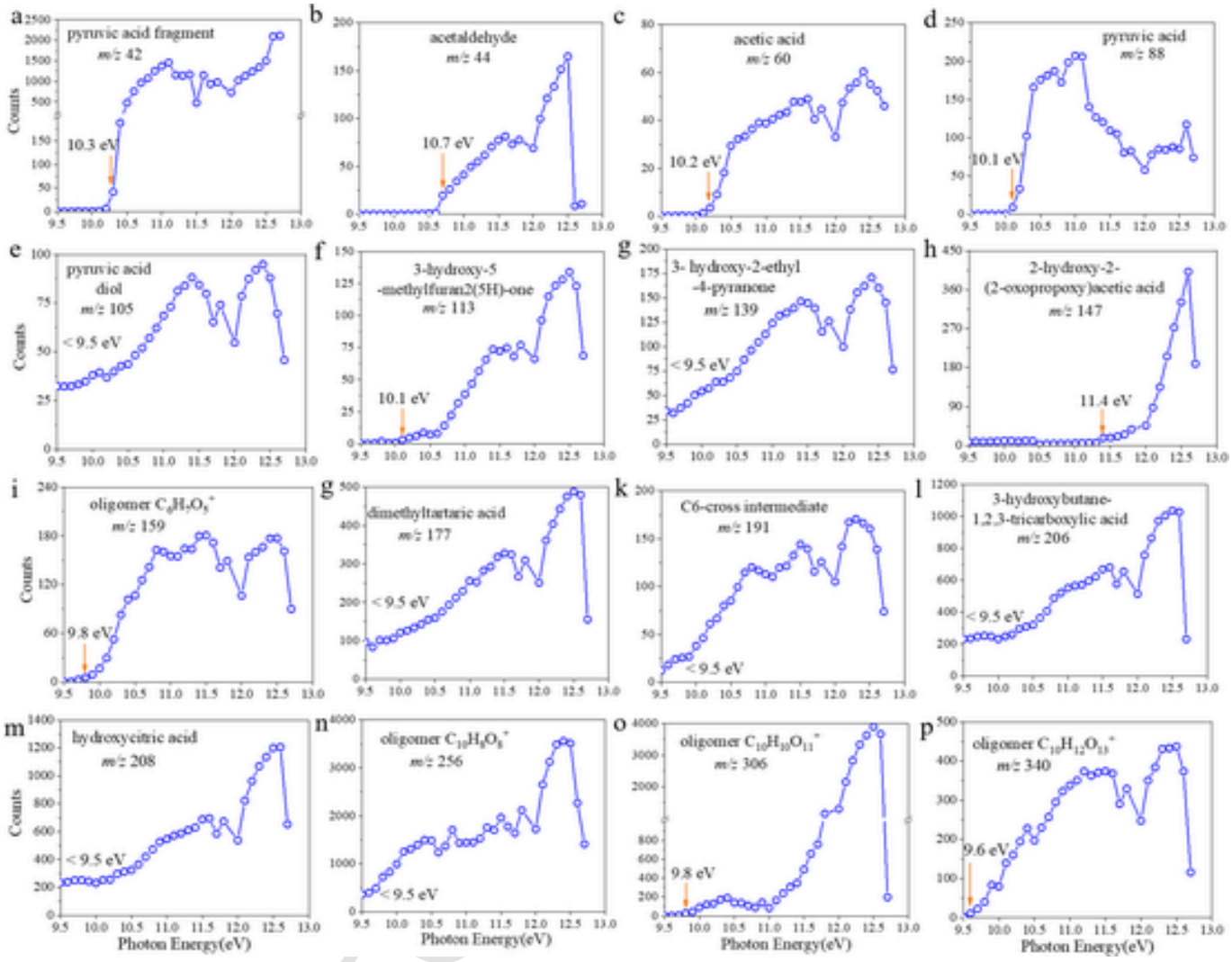


**Fig. 3.** Determination of appearance energies (AEs) of key products from the 4 h. UV aging observations of pyruvic acid.

cross-product) implies that PA is likely to form GA by decarboxylation, then it could undergo intersystem crossing via radical reactions at the a-l interface. Specifically, PA* can produce two radical pairs via proton-coupled electron transfer. After the protonation and deprotonation process, the radical anions and radical cations form lactic acid radical ($CH_3\dot{C}OHCOOH$), glycolic acid radical ($\dot{C}OHCOOH$), and oxyl radicals ($CH_3COCOO\bullet$ and $CHOCOO\bullet$), respectively. These radicals will combine with PA and GA molecules and formyl or acetyl radicals (decarboxylated by oxyl radicals) to form cross intermediate products like *m/z* 191. The precursor can undergo decarboxylation to form smaller products like *m/z* 147. The products shown in Fig. 4 marked as purple represent newly observed products in this work.

Another photochemical reaction route of PA is the generation of oligomers, which could contribute to aqSOA formation in the atmosphere (Reed Harris et al., 2014). In the aqueous phase, PA is known to spontaneously oligomerize to form a variety of oligomers via radical reactions (Rapf et al., 2017a). As expected, carboxylic acids and oligomers reported in previous studies were detected in this work, for instance, dimethyltartaric acid, oligomers *m/z* 159 $C_6H_7O_5^+$ and *m/z* 340 $C_{10}H_{12}O_{13}^+$ (see Table 1). Furthermore, newly discovered oligomers, including *m/z* 139 $C_7H_7O_3^+$, *m/z* 208 $C_6H_8O_8^+$, *m/z* 256 $C_{10}H_8O_8^+$, and *m/z* 306 $C_{10}H_{10}O_{11}^+$, indicate that other pathways may lead to aqSOA formation at the a – l interface. However, these products have not been reported in the bulk phase. Our results indicated that these oligomers are stable at the interface after 4 h of photolysis. Also, hydrolysis may also occur; and hydrated products may form in the bulk phase. Another possibility of the pathway of these oligomer formation, namely multi-radical reaction between PA, oxyl, and acetyl radicals can only occur during droplet evaporation at the interface, not has been observed in the bulk phase, as proposed in Fig. 4. Based on the results, the first step is that PA can generate radicals (e.g., $CH_3\dot{C}(OH)CO_2H$, $\dot{C}H_2C(O)CO_2H$) via photolysis in the aqueous phase (Rapf et al., 2017a). These radicals will form small carboxylic acid molecules and recombine to simple molecular oligomers. Then the preliminary products would generate oligomers of larger molecular weights via radical reaction or esterification in the presence of hydroxyl and carboxyl functional groups. The photochemical reactions are verified by the mass spectral analysis and comparisons of AE values between this work and published results. Several new products were detected, and the possible pathways were proposed to be following the radical reactions among PA itself, acetyl, and oxyl radicals for oligomer formation. The radical reactions could be induced within 1 h and last for several hours. For instance, some oligomers, such as *m/z* 139 $C_7H_7O_3^+$ and *m/z* 208 $C_6H_8O_8^+$, were observed in 1 h. While the intensities of these ions increased in 4 h. These long-carbon-chain products with moderately high Henry's law constants can partition into the aqueous phase as a formi-

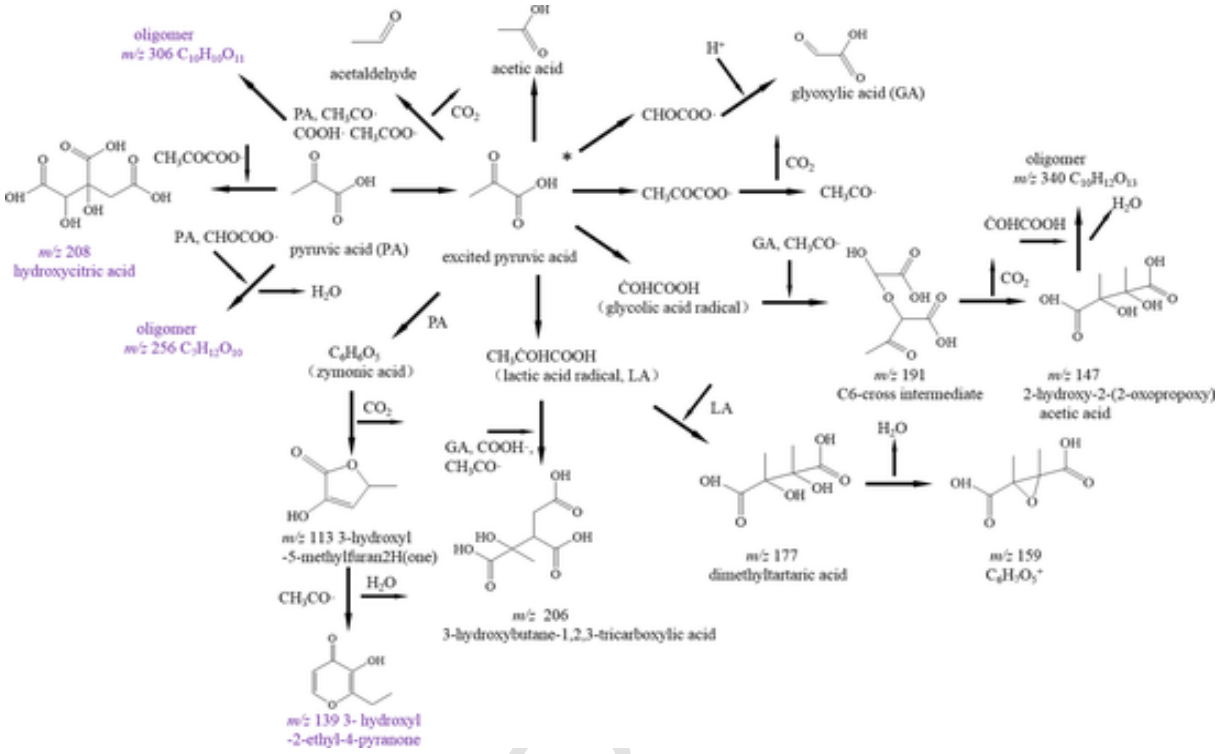


**Fig. 4.** Possible reaction pathways and structures of key products from the observations of the pyruvic acid after 4 h. UV aging. The postulated reactions are summarized as follows: 1) PA molecule is activated by light to form the singlet excited state PA*, 2) PA* produces radical anions and radical cations, 3) small carboxylic acid or simple molecular oligomers are formed via radical reactions, 4) the small molecule products generate large oligomers via radical reactions or esterification in the presence of hydroxyl and carboxyl.

dable source of aqSOA and contribute substantially to aqSOA during droplet evaporation. Specifically, dimethyltartaric acid (*m/z* 177) was generated by self-combination of two lactic acid radicals. The oligomers produced by esterification from dimethyltartaric acid (i.e., *m/z* 159 $C_6H_7O_5^+$). Moreover, PA and its excited radicals can react with subsequently generated radicals to form larger oligomers (i.e., *m/z* 206 $C_7H_{10}O_7^+$, *m/z* 139 $C_7H_7O_3^+$, *m/z* 208 $C_6H_8O_8^+$, *m/z* 256 $C_{10}H_8O_8^+$, 306 $C_{10}H_{10}O_{11}^+$) at the a-l interface. Moreover, carboxylic acids of larger molecular weights, for example, *m/z* 147 2-hydroxy-2-(2-oxopropoxy) acetic acid can form more complex oligomeric species (e.g., *m/z* 340 $C_{10}H_{12}O_{13}^+$) via photochemical oligomerization processes. The expanded reaction flowchart was summarized in Fig. 4. The newly observed products are highlighted in purple.

In terms of reaction time, oligomer formation is facilitated by longer photochemical processing time as shown in Fig. S3. Particularly, products like *m/z* 159 $C_6H_7O_5^+$ and *m/z* 191 $C_6H_7O_7^+$ could only be observed in long-time UV samples, namely, 24 h. and 4 h. samples. These results indicate that some PA photolysis and subsequent reactions, including photoinduced cross reactions and subsequent acetyl radical reactions might complete within several hours according to the resemblance of peak distribution between the 4 h. and 24 h. samples. As the PA photolysis was assumed to be a first-order reaction (Reed Harris et al., 2016), the photolysis reaction rate is inversely proportional to the PA concentration approximately. More products were observed, and the oligomer peaks have relatively higher normalized intensity in the 4 h. sample than in the 1 h. sample (Fig. S3). This finding suggests that PA photolysis could form oligomers at higher concentration over time. Higher intensity of dimethyltartaric acid (*m/z* 177) was observed compared to those of acetic acid (*m/z* 60) and oxo-products (*m/z* 191) as shown in Fig. 2. This indicates that the quantum yield of dimethyltartaric acid is higher than those of acetic acid and oxo-products under atmospheric irradiation because of the active production of excited triplet PA (Chen et al., 2022). Moreover, in the case of dissolved $O_2$, the ground state of $O_2$ could form singlet oxygen ($^1O_2$) by acquiring energy from the triplet exited state of an organic molecule (Chen et al., 2022; Zhang et al., 2019b). Because a dicarbonyl contains both ketone and carboxyl groups, PA can lead to remarkably enhanced production of $^1O_2$ compared with monocarbonyl organics (Chen et al., 2022). High concentration of $^1O_2$ may accelerate oligomers formation and initiate subsequent reactions to form larger oligomers based on the products generated by PA photolysis, corresponding to the high intensity of carboxylic acid and oligomers peaks observed in the 4 h. UV aged sample (see Fig. S3) (Kaur and Anastasio, 2017; Rapf et al., 2017b)."

The ambient pressure XPS (APXPS) has potential to study chemical processes at the a-l interface (Head and Schnadt, 2016; Starr et al., 2013). However, APXPS requires a specially built stand-alone instrument, currently limiting its access to users due to cost and availability. Also, it has not been used to study the SOA formation mechanism to the best of our knowledge (Zhang et al., 2022).

## 4. Conclusion

We performed in situ VUV SPI-MS analysis of UV treated PA samples enabled by the SALVI microreactor. The products and mechanism of PA photolysis reactions at the a-l interface are investigated by using the v-l interface via vacuum compatible microfluidics in this study. Different kinds of products are observed compared with results of bulk liquid results, demonstrating that the reaction pathways are different because of the active physicochemical properties at the a-l interface. Preliminary products, such as acetic acid and acetaldehyde, are affirmed by their AEs determined from the PIE curves. Moreover, the AE values for new products are assigned and their molecular structures deduced.

Our results suggest that PA firstly get activated to the excited state due to UV irradiation, then it could produce lactic acid radical, glycolic

CORRECTED

acid radical, oxyl radicals. PA can be decarboxylated to form acetaldehyde, acetic acid, and GA. The next step is that PA and GA could form cross products via photoinduced cross reactions with radicals. In addition, preliminary products could form complex oligomers with higher molecular weight via radical reaction by participation of hydroxyl and carboxyl functional groups. Another considerable source of aqSOA at the aqueous interface is via the radical reaction among PA itself, acetyl, and oxyl radicals. The mass spectral analysis shows that photochemical species and their yields increase as the aging time goes. These findings suggest that PA photolysis and subsequent radical reactions could be a significant mechanism of oligomer production, contributing to aqSOA formation of particles containing water.

These results have immediate implications in understanding the cause and aggregation of haze formation in the atmosphere. VUV photons provide an effective measure to study interfacial reactions of soluble VOCs based on the determination of mass spectral signatures and AEs. In summary, we gain new insights of PA a-l interfacial photolysis reactions, which are known as an important source of SOAs. In the atmosphere, the photochemistry of VOCs could occur in gas, aqueous, multiphase, and the a-l interface. The reaction pathways of VOCs at the interface and gas/aqueous phases are different, because the physicochemical properties at the aqueous surface are different from that in the bulk liquid or solid. Therefore, it is highly important to study the relevant reactions which could contribute to SOA formation at the a-l interface using various interfacial analysis methods like the novel liquid VUV SPI-MS technique presented in this work.

## CRediT authorship contribution statement

**Xiao Sui:** Writing – original draft, Methodology, Investigation, Formal analysis. **Bo Xu:** Writing – review & editing, Formal analysis, Data curation. **Oleg Kostko:** Writing – review & editing, Formal analysis, Data curation. **Xiao-Ying Yu:** Writing – review & editing, Writing – original draft, Validation, Supervision, Software, Resources, Project administration, Methodology, Investigation, Funding acquisition, Formal analysis, Data curation, Conceptualization.

## Declaration of competing interest

The authors declare that they have no known competing financial interests or personal relationships that could have appeared to influence the work reported in this paper.

## Data availability

The datasets generated for this study can be found in the article/Supplementary Material, further inquiries can be directed to the corresponding author.

## Acknowledgements

Funding for XS was provided by Natural Science Foundation of Shandong Province, grant number ZR2022QB137. Funding for XYY was supported by the strategic Laboratory Directed Research and Development (LDRD) of the Physical Sciences Directorate of the Oak Ridge National Laboratory (ORNL). ORNL is managed by UT-Battelle, LLC, for the U. S. Department of Energy (DOE) under contract number DE-AC05-00OR22725. This research used resources of the Advanced Light Source (ALS), a Department of Energy (DOE) Office of Science User Facility under con-tract no. DE-AC02-05CH11231. Programmatic support for BX and OK was from the Office of Basic Energy Sciences of the U.S. DOE under Contract No. DE-AC02-05CH11231 at the Lawrence Berkley National Laboratory (LBNL), through the Gas Phase Chemical Physics Program and Condensed Phase, Interfaces, and Molecular Sciences Program. The authors thank Miss Rachel Komorek, Dr. Jiachao Yu, and Dr. Tyler Troy for their assistance in device fabrication, sample preparation, and data analysis. The authors also thank Dr. Musa Ahmed of LBNL for support of this research and access to the ALS beamline.

This manuscript has been authored by UT-Battelle, LLC under Contract No. DE-AC05-00OR22725 with the U.S. Department of Energy. The United States Government retains and the publisher, by accepting the article for publication, acknowledges that the United States Government retains a non-exclusive, paid-up, irrevocable, world-wide license to publish or reproduce the published form of this manuscript, or allow others to do so, for United States Government purposes. The Department of Energy will provide public access to these results of federally sponsored research in accordance with the DOE Public Access Plan (http://energy.gov/downloads/doe-public-access-plan).

## Appendix A. Supplementary data

Supplementary data to this article can be found online at https://doi.org/10.1016/j.scitotenv.2024.172729.

## References

Ahmed, M., Kostko, O., 2020. From atoms to aerosols: probing clusters and nanoparticles with synchrotron based mass spectrometry and X-ray spectroscopy. Phys. Chem. Chem. Phys. 22, 2713–2737.

Altieri, K.E., Carlton, A.G., Lim, H.-J., Turpin, B.J., Sertzinger, S.P., 2006. Evidence for oligomer formation in clouds: reactions of isoprene oxidation products. Environ. Sci. Technol. 40, 4956–4960.

Bell, F., Ruan, Q.N., Golan, A., Horn, P.R., Ahmed, M., Leone, S.R., Head-Gordon, M., 2013. Dissociative photoionization of glycerol and its dimer occurs predominantly via a ternary hydrogen-bridged ion-molecule complex. J. Am. Chem. Soc. 135, 14229–14239.

Brown, M.A., Winter, B., Faubel, M., Hemminger, J.C., 2009. Spatial distribution of nitrate and nitrite anions at the liquid/vapor Interface of aqueous solutions. J. Am. Chem. Soc. 131, 8354–8355.

Chen, J., Miao, X.-N., An, T., 2022. Detection of excited triplet species from photolysis of carbonyls: direct evidence for single oxygen formation in atmospheric environment. Sci. Total Environ. 837, 155464.

Church, J.R., Vaida, V., Skodje, R.T., 2021. Kinetic study of gas-phase reactions of pyruvic acid with $HO_2$. J. Phys. Chem. A 125, 2232–2242.

Du, H., Qu, C., Liu, J., Chen, W., Cai, P., Shi, Z., Yu, X.Y., Huang, Q., 2017. Molecular investigation on the binding of cd(II) by the binary mixtures of montmorillonite with two bacterial species. Environ. Pollut. 229, 871–878.

Ervens, B., Turpin, B.J., Weber, R.J., 2011. Secondary organic aerosol formation in cloud droplets and aqueous particles (aqSOA): a review of laboratory, field and model studies. Atmos. Chem. Phys. 11, 11069–11102.

Eugene, A.J., Pillar-Little, E.A., Colussi, A.J., Guzman, M.I., 2018. Enhanced acidity of acetic and pyruvic acids on the surface of water. Langmuir 34, 9307–9313.

Fu, Y., Zhang, Y., Zhang, F., Chen, J., Zhu, Z., Yu, X.-Y., 2018. Does interfacial photochemistry play a role in the photolysis of pyruvic acid in water? Atmos. Environ. 191, 36–45.

Gao, S., Ng, N.L., Keywood, M., Varutbangkul, V., Biahrein, R., Nenes, A., He, J., Yoo, K.Y., Beauchamp, J.L., Hodyss, R.P., Flagan, R.C., Seinfeld, J.H., 2004. Particle phase acidity and oligomer formation in secondary organic aerosol. Environ. Sci. Technol. 38, 6582–6589.

Gasper, Gerald L., Takahashi, Lynelle K., Zhou, Jia, Musahid Ahmed, J.F.M., Hanley, L., 2010. Laser desorption Postionization mass spectrometry of antibiotic-treated bacterial biofilms using tunable vacuum ultraviolet radiation. Anal. Chem. 82, 7472–7478.

Griffin, R.J., 2005. Development and initial evaluation of a dynamic species-resolved model for gas phase chemistry and size-resolved gas/particle partitioning associated with secondary organic aerosol formation. J. Geophys. Res. 110.

Griffith, Elizabeth C., Carpenter, Barry K., Shoemaker, R.K., Vaida, V., 2013. Photochemistry of aqueous pyruvic acid. Proc. Natl. Acad. Sci. 110, 11714–11719.

Guzman, M.I., Colussi, A.J., Hoffmann, M.R., 2006. Photogeneration of distant radical pairs in aqueous pyruvic acid glasses. J. Phys. Chem. A 931–935.

Guzma'n, M.I., Colussi, A.J., Hoffmann, M.R., 2006. Photoinduced oligomerization of aqueous pyruvic acid. J. Phys. Chem. A 110, 3619–3626.

Haruta, T., Ikeda, Y., Konyuba, Y., Fukuda, T., Nishioka, H., 2019. Development of novel correlative light and electron microscopy linkage system using silicon nitride film. Microscopy 68, 189–193.

Head, A.R., Schnadt, J., 2016. UHV and ambient pressure XPS: potentials for mg, MgO, and $mg(OH)_2$ surface analysis. JOM 68, 3070–3077.

Huang, R.J., Zhang, Y., Bozzetti, C., Ho, K.F., Cao, J.J., Han, Y., Daellenbach, K.R., Slowik, J.G., Platt, S.M., Canonaco, F., Zotter, P., Wolf, R., Pieber, S.M., Bruns, E.A., Crippa, M., Ciarelli, G., Piazzalunga, A., Schwikowski, M., Abbaszade, G., Schnelle-Kreis, J., Zimmermann, R., An, Z., Szidat, S., Baltensperger, U., El Haddad, I., Prevot, A.S., 2014. High secondary aerosol contribution to particulate pollution during haze events in China. Nature 514, 218–222.

Ito, T., Bekki, K., Fujitani, Y., Hirano, S., 2019. The toxicological analysis of secondary

CORRECTED PROOF

organic aerosol in human lung epithelial cells and macrophages. Environ. Sci. Pollut. Res. Int. 26, 22747–22755.
Kaur, R., Anastasio, C., 2017. Light absorption and the photoformation of hydroxyl radical and singlet oxygen in fog waters. Atmos. Environ. 164, 387–397.
Komorek, R., Xu, B., Yao, J., Ablikim, U., Troy, T.P., Kostko, O., Ahmed, M., Yu, X.Y., 2018. Enabling liquid vapor analysis using synchrotron VUV single photon ionization mass spectrometry with a microfluidic interface. Rev. Sci. Instrum. 89, 115105.
Komorek, R., Xu, B., Yao, J., Kostko, O., Ahmed, M., Yu, X.Y., 2020. Probing Sulphur clusters in a microfluidic electrochemical cell with synchrotron-based photoionization mass spectrometry. Phys. Chem. Chem. Phys. 22, 14449–14453.
Kostko, O., Bandyopadhyay, B., Ahmed, M., 2016. Vacuum ultraviolet photoionization of complex chemical systems. Annu. Rev. Phys. Chem. 67, 19–40.
Lee, M.-T., Brown, M.A., Kato, S., Kleibert, A., Türler, A., Ammann, M., 2015. Competition between Organics and Bromide at the Aqueous Solution–Air Interface as Seen from Ozone Uptake Kinetics and X-ray Photoelectron Spectroscopy. Chem. Eur. J. 119, 4600–4608.
Lee, M.-T., Orlando, F., Artiglia, L., Chen, S., Ammann, M., 2016. Chemical Composition and Properties of the Liquid–Vapor Interface of Aqueous C1 to C4 Monofunctional Acid and Alcohol Solutions. Chem. Eur. J. 120, 9749–9758.
Lewis, T., Faubel, M., Winter, B., Hemminger, J.C., 2011. $CO_2$ capture in amine-based aqueous solution: role of the gas-solution interface. Angew. Chem. Int. Ed. Engl. 50, 10178–10181.
Li, M., Boothby, C., Continetti, R.E., Grassian, V.H., 2023. Size-Dependent Sigmoidal Reaction Kinetics for Pyruvic Acid Condensation at the Air–Water Interface in Aqueous Microdroplets. J. Am. Chem. Soc. 145, 22317–22321.
Lim, Y.B., Tan, Y., Perri, M.J., Seitzinger, S.P., Turpin, B.J., 2010. Aqueous chemistry and its role in secondary organic aerosol (SOA) formation. Atmos. Chem. Phys. 10, 10521–10539.
Lin, G., Sillman, S., Penner, J.E., Ito, A., 2014. Global modeling of SOA: the use of different mechanisms for aqueous-phase formation. Atmos. Chem. Phys. 14, 5451–5475.
McNeill, V.F., 2015. Aqueous organic chemistry in the atmosphere: sources and chemical processing of organic aerosols. Environ. Sci. Technol. 49, 1237–1244.
Mellouki, A., Wallington, T.J., Chen, J., 2015. Atmospheric chemistry of oxygenated volatile organic compounds: impacts on air quality and climate. Chem. Rev. 115, 3984–4014.
Nel, A., 2005. Air Pollution–Related Illness: Effects of Particles. Science 308, 804–805.
Perkins, R.J., Shoemaker, R.K., Carpenter, B.K., Vaida, V., 2016. Chemical equilibria and kinetics in aqueous solutions of Zymonic acid. J. Phys. Chem. A 120, 10096–10107.
Petters, S.S., Hilditch, T.G., Tomaz, S., Miles, R.E.H., Reid, J.P., Turpin, B.J., 2020. Volatility change during droplet evaporation of pyruvic acid. ACS Earth Space Chem. 4, 741–749.
Pruyne, J.G., Lee, M.-T., Fábri, C., Beloqui Redondo, A., Kleibert, A., Ammann, M., Brown, M.A., Krisch, M.J., 2014. Liquid–Vapor Interface of Formic Acid Solutions in Salt Water: A Comparison of Macroscopic Surface Tension and Microscopic in Situ X-ray Photoelectron Spectroscopy Measurements. J. Phys. Chem. C 118, 29350–29360.
Qi, L., Zhang, Z., Wang, X., Deng, F., Zhao, J., Liu, H., 2021. Molecular characterization of atmospheric particulate organosulfates in a port environment using ultrahigh resolution mass spectrometry: identification of traffic emissions. J. Hazard. Mater. 419, 126431.
Rapf, R.J., Perkins, R.J., Carpenter, B.K., Vaida, V., 2017a. Mechanistic description of photochemical oligomer formation from aqueous pyruvic acid. J. Phys. Chem. A 121, 4272–4282.
Rapf, R.J., Perkins, R.J., Yang, H., Miyake, G.M., Carpenter, B.K., Vaida, V., 2017b. Photochemical synthesis of oligomeric Amphiphiles from alkyl oxoacids in aqueous environments. J. Am. Chem. Soc. 139, 6946–6959.
Reader, J., Sansonetti, C.J., Bridges, J.M., 1996. Irradiances of spectral lines in mercury pencil lamps. Appl. Opt. 35, 78–83.
Reed Harris, A.E., Ervens, B., Shoemaker, R.K., Kroll, J.A., Rapf, R.J., Griffith, E.C., Monod, A., Vaida, V., 2014. Photochemical kinetics of pyruvic acid in aqueous solution. J. Phys. Chem. A 118, 8505–8516.
Reed Harris, A.E., Doussin, J.-F., Carpenter, B.K., Vaida, V., 2016. Gas-phase photolysis of pyruvic acid: the effect of pressure on reaction rates and products. Chem. Eur. J. 120, 10123–10133.
Reed Harris, A.E., Pajunoja, A., Cazaunau, M., Gratien, A., Pangui, E., Monod, A., Griffith, E.C., Virtanen, A., Doussin, J.F., Vaida, V., 2017. Multiphase photochemistry of pyruvic acid under atmospheric conditions. J. Phys. Chem. A 121, 3327–3339.
Samanta, B.R., Fernando, R., Rosch, D., Reisler, H., Osborn, D.L., 2021. Primary photodissociation mechanisms of pyruvic acid on S1: observation of methylhydroxycarbene and its chemical reaction in the gas phase. Phys. Chem. Chem. Phys. 23, 4107–4119.
Seidel, R., Thürmer, S., Winter, B., 2011. Photoelectron spectroscopy meets aqueous solution: studies from a vacuum liquid microjet. J. Phys. Chem. Lett. 2, 633–641.
Starr, D.E., Liu, Z., Havecker, M., Knop-Gericke, A., Bluhm, H., 2013. Investigation of solid/vapor interfaces using ambient pressure X-ray photoelectron spectroscopy. Chem. Soc. Rev. 42, 5833–5857.
Stephanou, E.G., 2005. The decay of organic aerosols. Nature 31.
Sui, X., Zhou, Y., Zhang, F., Chen, J., Zhu, Z., Yu, X.Y., 2017a. Deciphering the aqueous chemistry of glyoxal oxidation with hydrogen peroxide using molecular imaging. Phys. Chem. Chem. Phys. 19, 20357–20366.
Sui, X., Zhou, Y., Zhang, F., Zhang, Y., Chen, J., Zhu, Z., Yu, X.Y., 2017b. ToF-SIMS characterization of glyoxal surface oxidation products by hydrogen peroxide: a comparison between dry and liquid samples. Surf. Interface Anal. 50, 927–938.
Sui, X., Xu, B., Yao, J., Kostko, O., Ahmed, M., Yu, X.Y., 2021a. New insights into secondary organic aerosol formation at the air-liquid Interface. J. Phys. Chem. Lett. 12, 324–329.
Sui, X., Xu, B., Yu, J., Kostko, O., Ahmed, M., Yu, X.Y., 2021b. Studying interfacial dark reactions of Glyoxal and hydrogen peroxide using vacuum ultraviolet single photon ionization mass spectrometry. Atmosphere 12, 338.
Tsui, W.G., Rao, Y., Dai, H.L., McNeill, V.F., 2017. Modeling photosensitized secondary organic aerosol formation in laboratory and ambient aerosols. Environ. Sci. Technol. 51, 7496–7501.
Waxman, E.M., Dzepina, K., Ervens, B., Lee-Taylor, J., Aumont, B., Jimenez, J.L., Madronich, S., Volkamer, R., 2013. Secondary organic aerosol formation from semi- and intermediate-volatility organic compounds and glyoxal: relevance of O/C as a tracer for aqueous multiphase chemistry. Geophys. Res. Lett. 40, 978–982.
Winter, B., Faubel, M., 2006. Photoemission from Liquid Aqueous Solutions. Chem. Rev. 106, 1176–1211.
Xia, S.S., Eugene, A.J., Guzman, M.I., 2018. Cross photoreaction of glyoxylic and pyruvic acids in model aqueous aerosol. J. Phys. Chem. A 122, 6457–6466.
Yang, L., Yu, X.-Y., Zhu, Z., Thevuthasan, T., Cowin, J.P., 2011. Making a hybrid microfluidic platform compatible forin situimaging by vacuum-based techniques. J. Vac. Sci. Technol. A 29, 061101.
Yu, X.-Y., 2020. In situ, in vivo, and in operando imaging and spectroscopy of liquids using microfluidics in vacuum. J. Vac. Sci. Technol. A 38, 040804.
Yu, X.-Y., Liu, B., Yang, L., 2013. Imaging liquids using microfluidic cells. Microfluid. Nanofluid. 15, 725–744.
Zhang, F., Yu, X., Chen, J., Zhu, Z., Yu, X.-Y., 2019a. Dark air–liquid interfacial chemistry of glyoxal and hydrogen peroxide. NPJ Clim. Atmos. Sci. 2.
Zhang, F., Yu, X., Sui, X., Chen, J., Zhu, Z., Yu, X.-Y., 2019b. Evolution of aqSOA from the air-liquid interfacial photochemistry of glyoxal and hydroxyl radicals. Environ. Sci. Technol. 53, 10236–10245.
Zhang, F., Yu, X.-Y., Wang, Z., 2022. Analytical advances to study the air – water interfacial chemistry in the atmosphere. Trends Environ. Anal. Chem. 36, e00182.
Zhou, Y., Yao, J., Ding, Y., Yu, J., Hua, X., Evans, J.E., Yu, X., Lao, D.B., Heldebrant, D.J., Nune, S.K., Cao, B., Bowden, M.E., Yu, X.Y., Wang, X.L., Zhu, Z., 2016. Improving the molecular ion signal intensity for in situ liquid SIMS analysis. J. Am. Soc. Mass Spectrom. 27, 2006–2013.

CORRECTED PROOF